An Analytical Model for the Photodetection Mechanisms in High-Electron Mobility Transistors

Murilo A. Romero, M. A. G. Martinez, and Peter R. Herczfeld

Abstract—**The use of microwave high-electron mobility transistors (HEMT's) as photodetectors or optically controlled circuit elements have attracted interest. A model of the optical characteristics of HEMT's, which takes into account carrier transport as well as the quantum mechanical nature of the two-dimensional (2-D) electron gas channel, is presented. It is shown that the effect of illumination is equivalent to a shift in the gate to source bias voltage, referred to as the internal photovoltaic effect. The theoretical model is supported by experimental results that demonstrate that the HEMT photoresponse is a nonlinear function of light intensity with very high responsivity at low optical power levels.**

I. Introduction

THE MERGING of microwave and optical components on a single substrate is an area of growing interest. The high-electron mobility transistor (HEMT) is a viable candidate for the optical-microwave transducers because of its excellent microwave characteristics and compatibility with GaAs and InP technologies.

Since the 1980's, the photodetection mechanisms of HEMT's have been studied, motivated by the possibility of combining light detection and signal amplification in a single monolithic chip. Between 1982 and 1984 a Bell Laboratories research group demonstrated a series of HEMT-based photoconductive detectors ([1], [2] and references therein) with encouraging results. The device showed an impulse response with a full-width of half maximum (FWHM) of 27 ps. Similar experiments were reported by Umeda [3] and Fetterman [4], utilizing the optoelectronic sampling technique. Frequency-domain measurements [5]–[8], on the other hand, revealed a very significant low frequency optical gain, but the 3-dB bandwidth was in the low-MHz range. Also, some HEMT devices exhibit a negative photoresponse, a decrease of the drain current when illuminated, as reported by Chang *et al.* and Thomasin *et al.* [9], [10]. This occurs when there is significant electron trapping [11], [12].

The above discussion suggests that the positive photoresponse of HEMT's is comprised of two contributions: a slow component, responsible for the low frequency gain, and a fast component, produced by the direct collection of photogenerated electrons. The slow component determines the 3-dB bandwidth but will probably be negligible in time-domain measurements where the HEMT is excited by optical pulses as short as 5 ps.

The two principal attempts thus far to model the positive photoresponse of HEMT's are incomplete [13], [14]. Chakrabarti and co-workers [13] included the optical excitation in the Poisson equation, but did not solve the transport equations for the optically generated excess carriers and ignored the optical absorption in the GaAs layer. No gain mechanism was identified. The model advanced by de Salles [14] treats the transport mechanism of the excess carriers in the GaAs layer as photoconductive. The effect of bias voltages on the drain photocurrent is not considered and the model predicts a simple linear relation between the photoresponse and the incident optical power, which is variance with empirical observations.

The aim of this communication is to fulfill the need for a more comprehensive study of the physics of HEMT's transistors under illumination. Specifically, the low frequency gain mechanism and the dependence of the photoresponse on optical intensity are derived in terms of device parameters such as thicknesses and doping densities of the pertinent layers. The derivation, which takes into account the quantum nature of the two-dimensional (2-D) electron gas (2-DEG) channel, is comprised of solving the Poisson and transport equations for the optically generated carriers.

The organization of the paper is as follows. First, the dominant photodetection mechanism, backgating caused by accumulation of photogenerated holes in the GaAs buffer layer, is identified. Next, the experimental results are discussed and compared to the theory. Finally, the frequency response of the HEMT's is discussed. The results will show that HEMT's manifest optical gain up to a few hundred MHz, particularly at low optical intensities. It is proposed an alternative device configuration capable of extending the bandwidth while still attaining gain.

II. The HEMT Under Optical Illumination—Analytic Considerations

The energy band diagram of a conventional AlGaAs/GaAs HEMT under illumination is illustrated in Fig. 1. If the energy

Manuscript received July 22, 1996; revised August 26, 1996. This work was supported in part by Martin Marietta Electronics Laboratory and CNPq (Brazilian Research Council).

M. A. Romero is with the Electrical Engineering Department, University of São Paulo, São Carlos, SP, 13560, Brazil.

M. A. G. Martinez and P. R. Herczfeld are with the Center for Microwave-Lightwave Engineering, Drexel University, Philadelphia, PA 19104 USA.

Publisher Item Identifier S 0018-9480(96)08487-6.

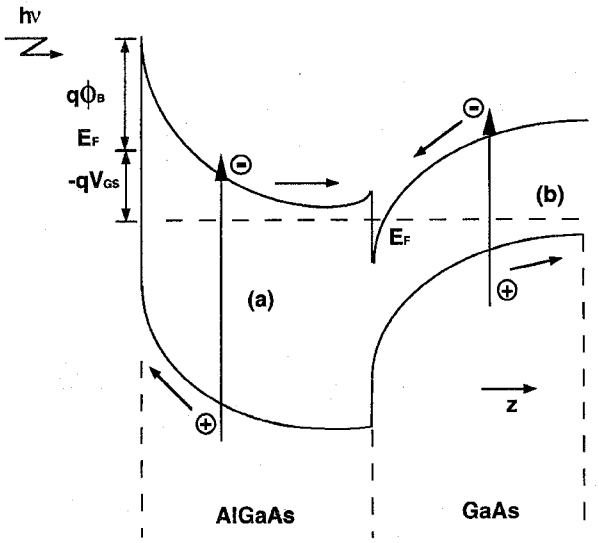

Fig. 1. AlGaAs/GaAs HEMT under optical illumination. (a) Photon absorption and electron-hole pair generation in the AlGaAs layer. (b) The corresponding situation for the GaAs layer, with the primary photoelectrons flowing from the GaAs buffer to the 2-DEG channel. The diagram is not drawn on scale. Typical AlGaAs and GaAs layers thicknesses are 400 Å and 1 μm, respectively.

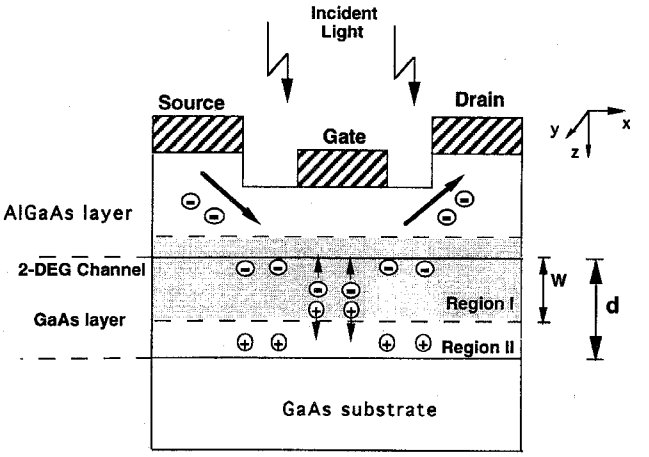

Fig. 2. Schematic representation of the photodetection process in a typical n^+AlGaAs/GaAs HEMT. Primary photoelectrons are collected by the drain while holes are driven toward the substrate and tend to accumulate in the neutral region of the nominally undoped GaAs buffer (region II). Charge neutrality is reestablished by electrons drawn from the external circuit and injected in the device from the source terminal.

of the incident photons is greater than the AlGaAs bandgap, absorption will occur in both layers. The photoeffects generated by light absorption in the AlGaAs layer have been addressed previously [15]. The photogenerated electron-hole pairs are separated by the built-in electric field created by the metal/semiconductor junction, which sweeps the electrons to the 2-D electron gas, while the holes enhance the gate current. In the presence of a large external resistor ($\approx$1 MΩ) in the gate biasing circuit, a significant photovoltage is developed across the Schottky barrier, which supplements the applied gate to source bias voltage. The usefulness of this effect is restricted by its slow response, set by the large RC time constant of the gate circuit.

The present work concerns the photoeffects associated with light absorption only in the GaAs buffer layer, which occur when the energy of the incident photons is less than the bandgap of the AlGaAs. In this event, a primary photoconductive current, consisting of electrons moving along the z-direction to the 2-DEG channel, arises. These electrons are then collected by the drain within a very short time period, corresponding to the transit time, which is in the range of tens of picoseconds.

The holes migrate toward the substrate and accumulate in the quasineutral region of the GaAs buffer. In steady-state, charge neutrality is reestablished by electrons drawn from the external circuit through the source contact, as illustrated in Fig. 2. The illumination acts as an "optical gate," controlling the flow of thermal equilibrium electrons in the 2-DEG channel. The positive charge build-up induces an open circuit photovoltage, called the *internal photovoltage*, which tends to forward bias the device. This positive photovoltage is superimposed on the applied gate to source voltage, V_{gs}. The mechanism is similar to the electrical or optical backgating observed in MESFET's [16], [17], and it is responsible for the high optical responsivity found in HEMT transistors [18].

The derivation presented in the ensuing sections considers the build-up of positive charge due to hole accumulation. This is followed by the calculation of the induced photovoltage and concludes with the computation of the drain output photoresponse as a function of device structure, bias point and incident optical power.

A. Hole Transport in the GaAs Layer

If the drain to source voltage is kept sufficiently small so that 2-D effects may be neglected, the continuity equation for holes in the GaAs material is

$$\frac{\partial}{\partial z}\left(D_p(E)\frac{\partial p'}{\partial z}\right)+\frac{\partial(p'v(E))}{\partial z}-\frac{p'}{\tau_p}+G(z)=0 \quad \text{for} \quad 0\le z\le d \tag{1}$$

where $D_p(E)$ is the hole diffusion coefficient, p' is the excess hole concentration, and $v(E)$ is the hole velocity in GaAs, τ_p is the excess carrier lifetime. The optical generation rate is $G(z)=\alpha F exp[-\alpha z]$, where F is the photon flux reaching the GaAs layer and α is the wavelength dependent absorption coefficient.

Equation (1) is solved employing the depletion approximation. The GaAs layer is divided into two regions, as shown in Fig. 2. In the space-charge region (region I) the electric field is high enough for the carriers to move at the saturation velocity v_s, in the z-direction. Since the carrier transit time is very short, recombination can be neglected. Furthermore, when a high-field condition exist, the mobility and the diffusion coefficient are considerably decreased [19]. Thus, diffusion is neglected in the space-charge region and (1) reduces to

$$\frac{v_s\partial p'}{\partial z}+G(z)=0, \quad \text{for} \quad 0\le z\le W.$$

Therefore, the total photogenerated hole density is

$$p' = \frac{-1}{v_s}\int_0^W G(z)\,dz = \frac{F}{v_s}[1 - e^{\alpha W}]$$

where, under strong inversion, the depletion width W is written as [20]

$$W = \sqrt{\frac{4\varepsilon_1 \beta \ln(N_a/n_i)}{qN_a}}.$$

In the above expression ε_1 is the dielectric permitivity of GaAs, β is the thermal voltage kT/q, N_a is the background unintentional acceptor density, and n_i the intrinsic carrier concentration in the GaAs layer. The photogenerated holes produce a photoconductive current flowing from the buffer to the substrate

$$J_{pr} = qv_s p' = qF[1 - \exp(-\alpha W)]. \tag{2}$$

In the quasineutral region, the electric field is very small and carrier drift is insignificant [19]. Equation (1) becomes

$$D_p \frac{\partial^2 p'}{\partial z^2} - \frac{p'}{\tau_p} + G(z) = 0 \quad \text{for} \quad W \le z \le d \tag{3}$$

where D_p represents the low field diffusion coefficient. The boundary conditions are: $p' = F/v_s[1-\exp(-\alpha W]$ at $z = W$, which implies charge continuity at the edge of the depletion region, and $dp'/dz \approx 0$ at $z = d$, which implies negligible recombination velocity at the semi-insulating substrate.

The solution of (5), subject to these boundary conditions, is

$$p'(z) = \frac{F}{\cosh\left[\dfrac{d-W}{L_p}\right]}\left\{\frac{\alpha\tau_p}{\alpha^2 L_p^2 - 1}\left[e^{-\alpha W}\cosh\left(\frac{d-z}{L_p}\right) - e^{-\alpha z}\cosh\left(\frac{d-W}{L_p}\right) - \alpha L_p e^{-\alpha d}\sinh\left(\frac{z-W}{L_p}\right)\right] + \frac{1}{v_s}[1 - e^{-\alpha W}]\cosh\left(\frac{d-z}{L_p}\right)\right\} \tag{4}$$

where $L_p = (D_p\tau_p)^{1/2}$ is the diffusion length. The excess carrier distribution in the neutral region of the GaAs buffer layer, a linear function of the photon flux, is now fully determined. The total number of holes in the quasineutral GaAs region is

$$P = \int_V p'(z)\,dV \tag{5}$$

where V is the volume of the quasineutral region. In the limit where this volume vanishes ($d - W \approx 0$) all photogenerated holes will be swept toward the substrate. In this event, the high-resistivity of the semi-insulating substrate will cause hole accumulation at the buffer/substrate interface. The steady-state concentration per unit area, Δp_i, reduces to

$$\Delta p_i = \int_0^W G(z)\,dz = F\tau_p[1 - e^{-\alpha W}] = \frac{\tau_p J_{pr}}{q}. \tag{5.a}$$

B. The Internal Photovoltaic Effect

The total number of holes accumulated in the buffer, given in (4), will have to be balanced by an increase in the 2-DEG electron concentration. These carriers are drawn from the external circuit, as the charge neutrality requires

$$P = \int_A \Delta n\,dA \tag{6}$$

where Δn is the increase in carrier concentration per unit area in the 2-DEG channel. This positive charge build-up alters the potential profile in the device, generating a positive photovoltage, V_{ph}, across the GaAs layer. V_{ph} is calculated via the capacitance C_{cb}, which relates the band-bending, V_{cb}, in the GaAs layer to the total charge Q

$$C_{cb} = \left|\frac{\partial Q}{\partial V_{cb}}\right| = \frac{\varepsilon_1}{W} + q^2\frac{\partial n_s}{\partial E_f}. \tag{7}$$

The first term in (7) is the usual depletion capacitance. The second dominating term is due to the 2-DEG electrons. The variation in band-bending ∂V_{cb} is identified as the induced photovoltage. In the strong inversion regime the depletion component can be neglected [19]. Then, using (7), one obtains

$$qV_{ph} = \Delta E_f. \tag{8}$$

The induced photovoltage is the shift of the quasi-Fermi level, a consequence of the illumination causing an increase in the carrier concentration. Since the induced photovoltage is governed by the carrier statistics

$$n_s = DKT\sum_{i=0}^{1}\ln[1 + e^{E_f - E_i/kT}]. \tag{9}$$

The photovoltage is computed by imposing charge neutrality (6) and calculating the electron quasi-Fermi energy level shift, from the numerical solution of (9). This solution is described in the literature [21] for conventional AlGaAs/GaAs HEMT's. However, since the transistors available for experimental studies were pseudomorphic devices, the existing formulation [21] was extended to accommodate these structures. Specifically, the carrier concentration as a function of Fermi level energy, shown Fig. 3, is obtained by treating the InGaAs layer as a square-well in the presence of an electric field [22], and solving (9) in accordance with the derivation provided in the Appendix.

The dependence of the photovoltage on optical power can be written in a compact form by using (5), (8), and (9). Since p' is a function only of the z coordinate, one obtains

$$\int_W^d p'(z,F)\,dz = n_{s1} - n_{so} = \Delta n(F) = DkT\sum_{i=0}^{1}\ln\left[\frac{\sigma_i + e^{qV_{ph} - \Delta E_i/kT}}{1+\sigma_i}\right] \tag{10}$$

where n_{so} and n_{s1} represent the dark and illuminated 2-DEG carrier concentration, $D = m/\pi\hbar^2$ is the two-dimensional density of states, ΔE_i is the energy shift of ith subband within the channel (Stark shift), caused by illumination, and the number of occupied subbands was taken as two ($i = 0$

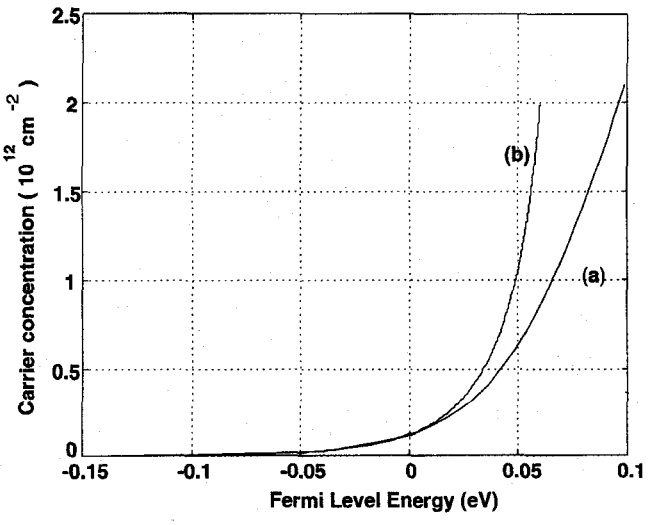

Fig. 3. Carrier concentration as a function of the Fermi level energy: (a) $L_w = 50$ Å and (b) $L_w = 90$ Å, where L_w represents the InGaAs layer thickness of a pseudomorphic HEMT structure. The zero reference level is taken as the bottom of the conduction band in the 2-DEG channel.

and 1). The constant σ_i is defined as $\sigma_i = \exp(E_i - E_f)/kT$ in the unilluminated state. It is related to the gate to source bias voltage and it is typically of the order of unity. When the GaAs buffer region is fully depleted (5a) is replaced by (5), and the left-hand side of (10) reduces to $\Delta p_i = n_{s1} - n_{so}$.

Finally, the photovoltage determined by (10) leads to a photoresponse (ΔI_{ds}), the difference between the illuminated ($I_{\rm ill}$) and dark (I_d) drain currents, given by

$$I_{\rm ph} = \Delta I_{ds} = I_{\rm ill} - I_d = g_m V_{\rm ph} \tag{11}$$

where g_m is the transconductance of the device.

A limiting case for very low optical power levels is obtained by simplifying (10). First, we neglect the Stark shift and assume low bias (only the first subband is occupied). Then, $\exp[qV_{\rm ph}/kT]$ is expanded in a Taylor series for small photovoltages (low light intensities). This results in an equation of the form $\ln(1+x)$ where $x = (qV_{\rm ph}/kT)[1/(1+\sigma_1)]$. For small values of x this expression is further simplified, $\ln(1+x) \approx x$, leading to the relation

$$V_{\rm ph} = \frac{(1+\sigma_o)\int_W^{d_1} p'(z)\,dz}{qD} = \frac{(1+\sigma_o)\kappa F \tau_p}{qD} \tag{12}$$

where the constant κ results from the integration of (5). Thus, for low intensities, $V_{\rm ph}$ is linearly proportional to the photon flux. The quantum efficiency in this case is

$$\eta = \frac{I_{\rm ph}}{qFA_i} = \frac{g_m(1+\sigma_o)\kappa\tau_p}{q^2 D A_i} \gg 1.$$

A long hole lifetime ($\approx$1.0 μs) results in a large optical gain (η in excess of 10^3), and the device performs as a photosensor-amplifier. The gain is optimized by biasing the device for maximum transconductance and reducing the illuminated area A (i.e., increasing the photon density per unit area by focusing the optical beam). An enlargement in interelectrode spacing will not result in improved performance.

Another limiting case results for high light intensities. Assuming again that only the first subband is occupied, we rewrite (9) as

$$n_s = DkT(1 + e^{E_f - E_0/kT}).$$

For $E_f - E_o \ll kT$ and using (10) for $V_{\rm ph}$, one gets

$$V_{\rm ph} - \frac{\Delta E_o}{q} \approx V_{\rm ph} = \frac{kT}{q}\ln\left[1 + \frac{\Delta n}{n_{so}}\right] = \frac{kT}{q}\ln\left[1 + \frac{F}{F_o}\right]. \tag{13}$$

This equation imply a logarithmic dependence of $V_{\rm ph}$ on the photon flux F, which tend to level off at high optical powers. The parameter F_o ascertains the onset of the saturation mechanism and is obtained from the charge neutrality and the value of Δn. It can be written

$$F_o = \frac{n_{so}}{\tau_p \kappa}.$$

F_o is inversely proportional to the hole lifetime and increases for larger values of n_{so} (larger V_{gs}). For a hole lifetime of 0.5 μs and a spot size of about 100 μm, saturation of the photoresponse starts for optical power inputs as low as 20 μW (the estimates were based on typical values of the GE structure described in Section III). Note that (13) was derived for a nondegenerated case, the logarithmic response is also valid for a degenerate (i.e., $E_f - E_o$ larger than kT) channel.

The source of the saturation is the nonlinear relation between the photovoltage and the accumulated hole concentration. From (8) and (11) we obtain

$$I_{\rm ph} = \Delta I_{ds} = \frac{g_m}{q}\Delta E_f.$$

Rewriting $\Delta I_{ds}/\Delta E_f = (\Delta I_{ds}/\Delta n_s)(\Delta n_s/\Delta E_f)$, it follows that

$$\frac{\Delta I_{ds}}{\Delta n_s} = \frac{g_m}{q}\frac{\Delta E_f}{\Delta n_s}. \tag{14}$$

Accordingly, the increment in drain current is proportional to the slope of the $E_f - n_s$ relation, which is depicted in Fig. 3 for pseudomorphic HEMT's with InGaAs channel widths of 50 and 90 Å. Since the slope reduces as n_s increases, saturation takes place. The saturation is more pronounced for devices with wider channels.

III. Experimental Results

In this section the theoretical predictions are compared with the experiments for the photoresponse of two HEMT devices. The first structure investigated was an InGaAs channel pseudomorphic HEMT fabricated by General Electric. The device was grown by MBE atop of a semi-insulating LEC substrate and include the following layers: 1 μm of undoped GaAs, 90 Å of undoped $In_{0.17}Ga_{0.83}As$ (the quantum-well channel), 45 Å of undoped $Al_{0.17}Ga_{0.83}As$ spacer, 400 Å of planar-doped $Al_{0.17}Ga_{0.83}As$, and 350 Å of highly doped GaAs as a cap layer. The external geometry comprises of a gate with length 0.25 μm and width 200 μm, and gate to source and gate to drain spacings of 0.5 and 0.6 μm, respectively.

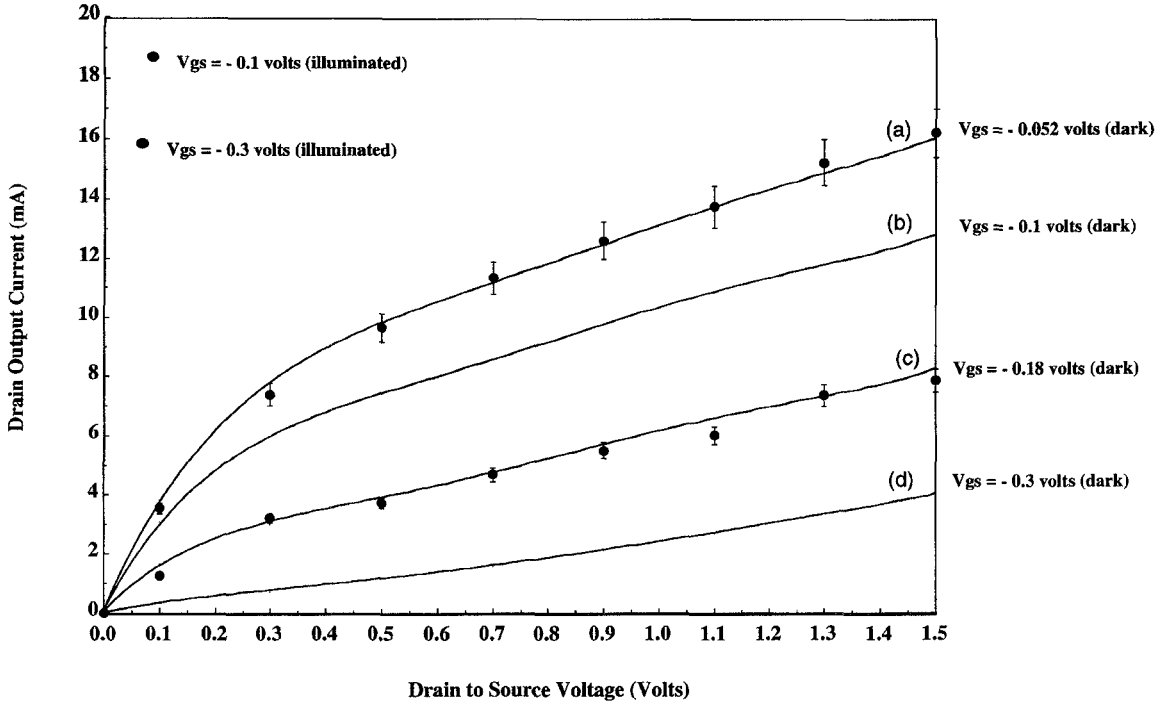

Fig. 4. I–V characteristics for the InGaAs pseudomorphic structure under dark and illuminated conditions. Starting with a particular gate to source bias point (solid curves (b) $V_{gs} = -0.1$ and (d) -0.3 V are shown) the change in drain current caused by illumination (the dots) can be retraced by increasing V_{gs}, solid curves (a) and (c). The equivalent gate photovoltage $V_{\rm ph}$ is of 48 and 120 mV, respectively.

The second structure studied was fabricated by Raytheon. The active device consists of 150 Å of planar doped InGaAs quantum-well channel (Si doped 5×10^{12} cm^{-2}) sandwiched between undoped GaAs barriers (few hundred Å thick). This HEMT has two 100 μm gate fingers and two source pads connected to the backside ground plane by via holes. The source to drain spacing is 2.5 μm and the gate (0.25 μm) is centered between source and drain contacts.

The devices were mounted in a coplanar waveguide microwave carrier in a common-source configuration. Illumination was provided by a pig-tailed Ortel SL-1020 semiconductor laser diode ($\lambda = 0.83$ μm), so that the AlGaAs was transparent to the incident optical energy. The output multimode fiber (core and cladding diameters of 62.5 and 125 μm, respectively) is held 500 μm above the device by a micropositioner. A video-camera/video-display apparatus monitors the fiber position to assure that optimum fiber placement is maintained. A variable optical attenuator controls the photon flux intensity illuminating the device.

In the subsequent discussions, the optical power is measured at the output of the pigtailed laser and the coupling efficiency is measure of how much of the light is absorbed in the active area of the device. Taking into consideration the geometry of the devices, reflections at the interfaces and the Gaussian spatial profile of the light beam, is estimated to be of the order of 2%.

A. Drain Photoresponse as a Function of Gate to Source Voltage

As stated earlier, the stored holes control the drain current, and the HEMT respond to the optical illumination as if a photoinduced gate voltage $V_{\rm ph}$ was applied to the device terminals. Generally, an external observer will perceive the effect of the optical illumination as a shift in the effective gate to source bias point from the dark value V_{gs} to the illuminated value V'_{gs} is

$$V'_{gs} = V_{gs} - V_{\rm ph}.$$

The incident light may be viewed as an additional terminal that optically controls the device operation. The dark and illuminated dc I–V characteristics of the General Electric device, depicted in Fig. 4, provide the empirical verification of this assertion.

First, the dark I–V characteristics were measured at fixed gate bias voltages (the solid curves (b) and (d) in Fig. 4, where V_{gs} was set equal to -0.1 V and -0.3 V, respectively). Next, the device was illuminated with 1 mW of optical power and the I–V curve was remeasured while holding the bias constant at the previous set levels (the dots with error bars in Fig. 4). This produces a shift in the I–V characteristics. Then, the optical radiation was turned off and the previously created illuminated I–V curves were reproduced by proper adjustment of the gate bias voltage (the solid curves (a) and (c) in Fig 4). For instance, consider the two top curves of Fig. 4: starting from $V_{gs} = -0.1$ V, identical current increase is obtained (within experimental error) by illuminating the device or readjusting the gate to source bias voltage by 48 mV, which is identified as the photovoltage $V_{\rm ph}$. By systematically repeating this procedure at different bias points and light intensities, one can empirically map the photovoltage and relate it to the gate to source bias voltage. Table I lists the theoretical and experimental photovoltages at an optical intensity of 1 mW.

TABLE I
THEORY AND EXPERIMENT FOR THE PHOTOVOLTAGE VERSUS GATE-TO-SOURCE BIAS FOR THE GENERAL ELECTRIC HEMT

Gate to Source Bias	Vph - experimental	Vph - theoretical
0.0 volts	35 mV	39 mV
- 0.1 volts	48 mV	50 mV
- 0.2 volts	68 mV	63 mV
- 0.3 volts	120 mV	92 mV

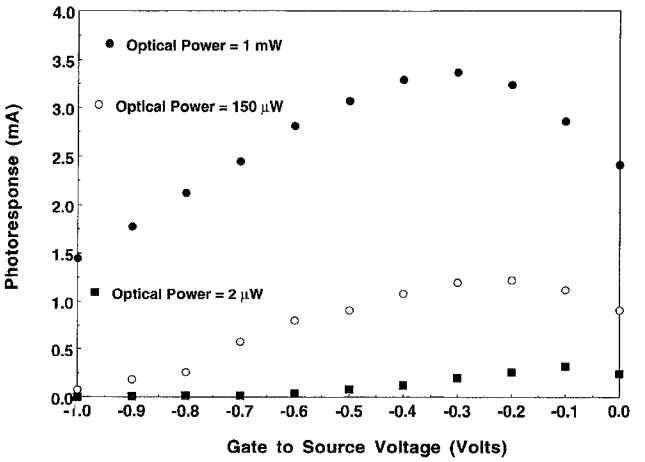

Fig. 5. Experimental drain current photoresponse versus gate to source bias voltage with the incident optical power as a parameter.

To generate the theoretical values for Table I we assumed a uniformly illuminated device and a spot size of 100 μm. To compute the quasi-Fermi level shift several steps are taken. First, the dark carrier concentration, n_{so}, is extracted from the measured I–V characteristics using the saturation velocity in the channel (10^7 cm/s). Then, from (9) the dark Fermi level is calculated. Since the depletion width is larger than the GaAs layer thickness, the approximation $\Delta n = \Delta p_i$ (5a) was introduced. Once Δn and n_{so} are known the carrier concentration under illumination, n_s, is determined. Finally, the change in Fermi level, which is directly proportional to the photovoltage, was found using (9).

The model yields very good agreement for large values of V_{gs}. When the gate bias is lowered, however, the strong inversion approximation (Section II-A) is no longer valid, and the theoretical model tends to underestimate the photoresponse.

It is noted that the drain photoresponse is not a monotonic function of the gate bias and it reaches a maximum for a particular value of V_{gs}, because of the bell-shaped g_m-V_{gs} relation in HEMT's. This is experimentally confirmed in Fig. 5. Furthermore, the gate voltage that optimizes the photoresponse is dependent on the incident optical power. For low optical intensities the photovoltage is small and the maximum photoresponse (the product $g_m V_{\rm ph}$) is approximated by the voltage that maximizes the transconductance, $V_{gs} = 0.0$ V for this device.

It should be stressed that the concept of an equivalent gate photovoltage, discussed in this section, also holds for the Raytheon transistor, as well as for all the other devices tested [12].

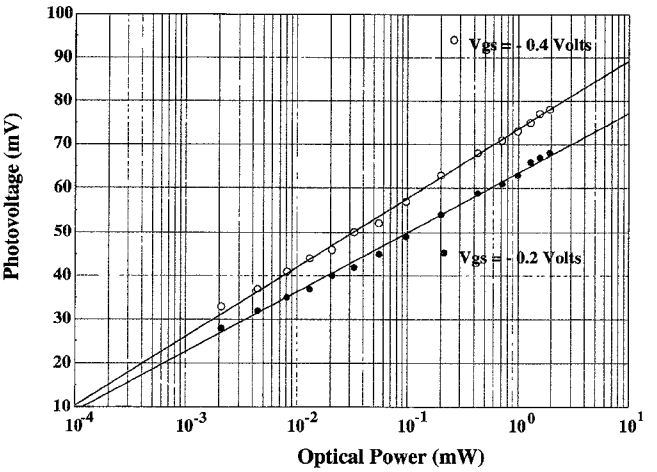

Fig. 6. Experimental photovoltage versus optical power for the Raytheon HEMT. The gate to source voltage was used as a parameter.

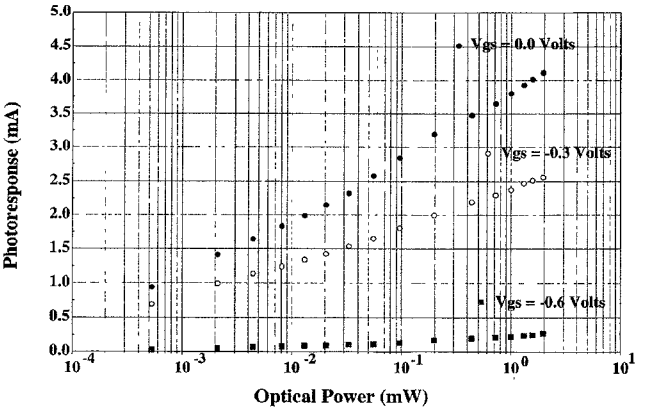

Fig. 7. Experimental drain photoresponse versus optical power for the Raytheon HEMT. The gate to source voltage was used as a parameter and V_{ds} is fixed at 1.0 V.

B. Drain Photoresponse as Function of Light Intensity

On the basis of (13), a logarithmic relation between the equivalent photovoltage $V_{\rm ph}$ and the light intensity is expected. This assertion is substantiated by the experimental results shown in Fig. 6. Three orders of magnitude variation in light intensity (from 2μW to 2 mW) alters the photovoltage from 33 to 78 mV. The results also reveal that the photovoltage increases as V_{gs} becomes more negative.

The photoresponse, like the photovoltage, varies logarithmically with intensity, as depicted in Fig. 7. The photoresponse drops markedly as the device approaches pinch-off because of the lower transconductance.

The experimental and analytic photoresponse for the GE HEMT is plotted in Fig. 8. The photoresponse starts to saturate at about 50 μW of optical intensity, in good agreement with our analytical prediction. In this calculation the only fitting parameter was the lifetime τ_p, which is related to the characteristic turn-off time of the internal photovoltaic effect. The value used, 0.6 μs, is consistent with a measured bandwidth of 1–2 MHz at this bias level (Section III-C).

The responsivity ($R = I_{\rm ph}/P_{\rm opt}$) as a function of the incident optical power for the GE HEMT and for a refer-

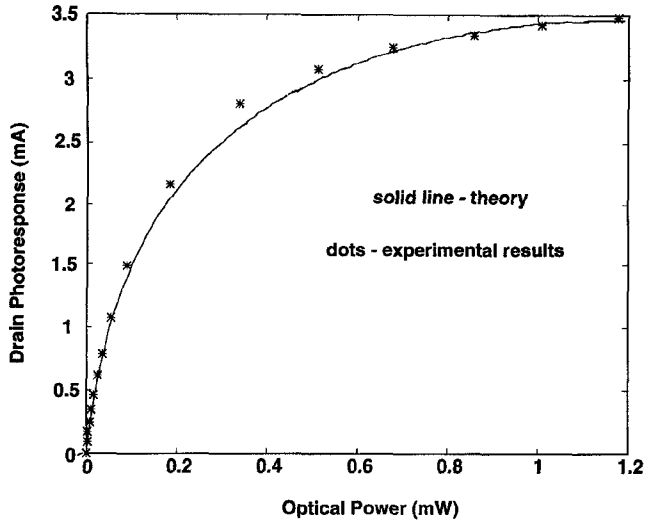

Fig. 8. Theory (solid line) versus experiment (dots) for the photocurrent—optical power relation at the bias point $V_{gs} = -0$ 1 V and $V_{ds} = 1.0$ V. The transconductance gm was experimentally obtained as 70 mS. The hole lifetime is 0.6 μs and the dark carrier concentration nso is 1.92×10^{11} cm^{-2}.

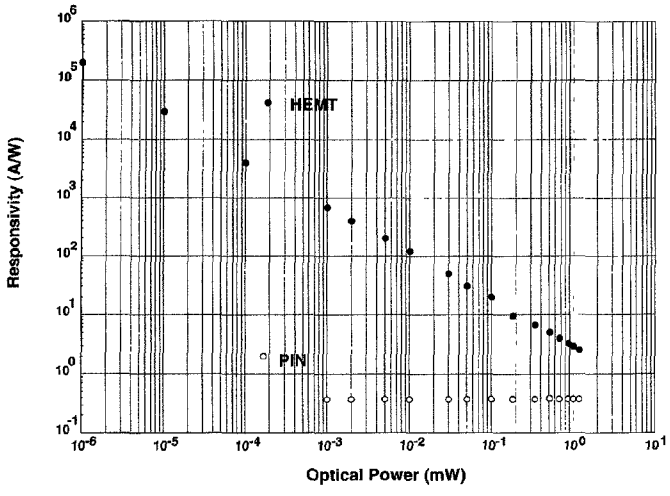

Fig. 9. Experimental responsivity versus optical power for the GE HEMT ($V_{gs} = 0.0$ V, $V_{ds} = 1.5$ V) and reference p-i-n photodiode.

ence PIN photodiode is shown in Fig. 9. The p-i-n has a linear response with a constant responsivity of 0.38 A/W. The responsivity of the HEMT, which is proportional to the external quantum efficiency, manifests a very large gain at low intensities, exceeding 100 A/W for optical powers below 10 μW. The GE HEMT yielded a drain current of more than 0.1 mA at an optical illumination of one nanowatt, which corresponds to a responsivity in excess of 10^5 A/W. Even for optical power levels as high as 1 mW the responsivity is 3.5 A/W, one order of magnitude higher than the p-i-n. It need to be emphasized that the light intensity referred to in the experimental curves is the available power at the output of the laser. The responsivity results are even more remarkable if one considers the small optical coupling efficiency of HEMT's. The device is an excellent low-frequency optical sensor.

C. Frequency Response

The frequency response of the GE device at three different optical input levels is shown in Fig. 10. A high-speed p-i-n is taken as the 0-dB reference level, thereby accounting for the laser response. The bandwidth is in the range of a few MHz and no optical gain is registered because the device is deeply biased in pinch-off. A different case is depicted in Fig. 11, which shows optical gain as a function of intensity for $V_{gs} = 0.0$ V at different modulation frequencies. These curves suggest that the HEMT performs better then the p-i-n at low optical input levels and at low modulation frequencies.

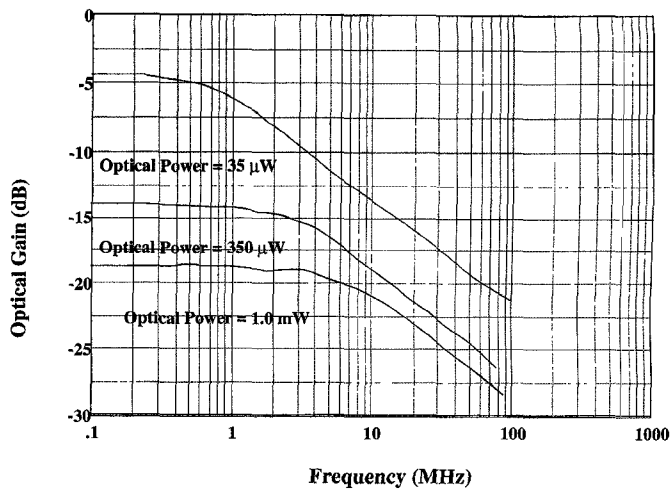

Fig. 10. Frequency response as a function of light intensity for the MODFET. The gate to source bias voltage is $V_{gs} = -0.9$ V.

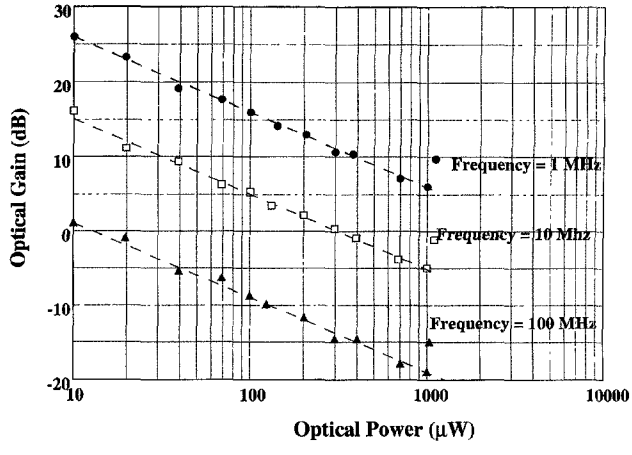

Fig. 11. Experimental RF optical gain as a function of light intensity with the frequency as a parameter.

The reason for the slow response is the long hole lifetime, which provides for the high gain, but at the expense of speed. This unusually long lifetime is a result of the spatial separation of photogenerated electrons and holes, which decreases the recombination probability. Similarly long lifetimes were reported by Garmire *et al.* in a metal/AlGaAs/GaAs Schottky diode [23].

The picosecond response reported by previous investigators [1]–[4] using pulsed measurements are attributed to the small primary photoconductive current which does not provide for gain. To increase the speed of the photovoltaic effect the hole lifetime must be reduced. Specifically, the task is to extend the bandwidth without critically sacrificing the gain. This can be

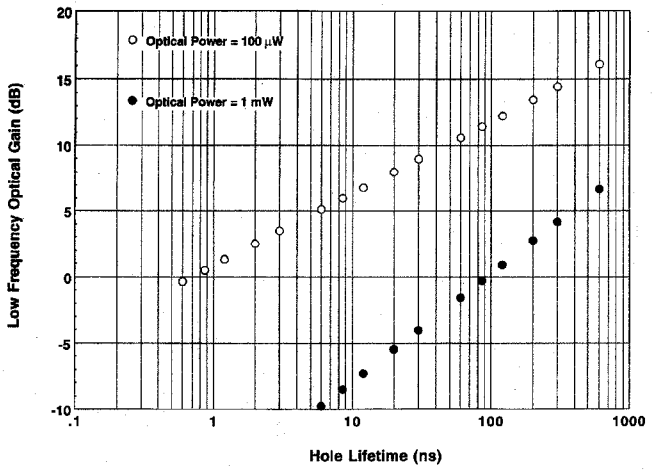

Fig. 12. Simulated low frequency optical gain versus hole lifetime for 100 μW and 1 mW of incident optical power.

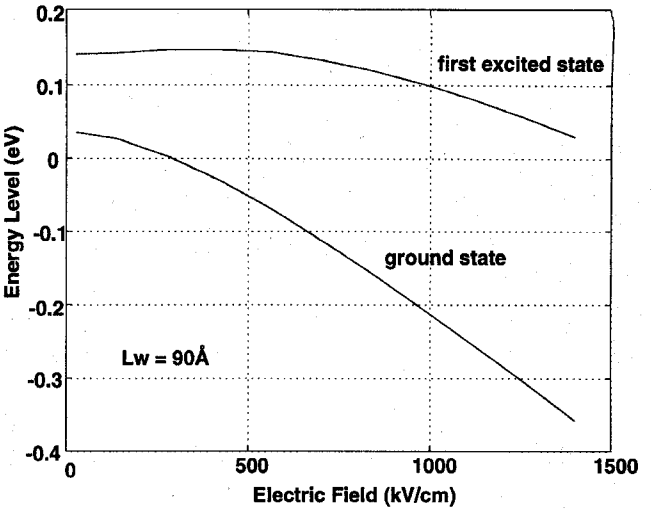

Fig. 13. Subband energy values as a function of the built-in electric field: (a) ground state and (b) first excited state. The well thickness is 90 Å for the General Electric pseudomorphic HEMT.

accomplished by the introduction of a "hole-sink" [2], whereby the excess holes are extracted from the GaAs layer via an additional terminal positioned at the substrate.

The calculations showing the effect of reduced hole lifetime on the low frequency optical gain is depicted in Fig. 12. At high light intensities, incident optical power of 1 mW or above, the improvement is insignificant because of saturation. At low light intensities (100 μW or less) the HEMT performs better. Specifically, at input levels of 100 μW or less the HEMT outperforms the p-i-n at frequencies up to 300 MHz.

IV. Conclusion

Current optical links utilize p-i-n and/or MSM photodiodes. In these two-terminal devices the optical gain is of the order of unity and the photocurrent increases linearly with the optical power. The HEMT's constitute a different class of photodetectors, where the optically generated carriers control the flow of the thermal equilibrium electrons. The light acts as an additional terminal, via the shift of the gate-to-source bias point, through which the performance of the device can be controlled. This provides an additional degree of freedom, that conventional photodiodes do not possess.

Regarding the photodetection performance, the devices are characterized by a logarithmic dependence on light intensity and have an extremely high quantum efficiency at low light intensities. The bandwidth, however, is in the low MHz range. Reducing the hole accumulation via a "hole sink" would enhance the gain bandwidth product. The utilization of the HEMT as a photodetector is limited to applications where moderate bandwidth, high sensitivity, and low power consumption are important, such as interconnects in digital hardware.

Appendix

The Appendix is concerned with obtaining the eigenvalues in the well of a pseudomorphic HEMT. Models for conventional AlGaAs/GaAs devices use the infinite triangular well approximation, where the solution of the Schroedinger equation yields eigenstates described by Airy functions from which the E_f-n_s relationship is obtained [21].

However, for pseudomorphic structures, only numerical models are reported [24], where the Schroedinger and Poisson equations are solved self-consistently. Although accurate, these models are computer intensive and do not provide for a physical insight into the photodetection mechanisms in HEMT's. Alternatively, one can extend the formulation advanced by Drummond *et al.* [21] to pseudomorphic devices. The InGaAs channel is treated as a square-well subject to a built-in electric field. The potential profile is described as

$$V(z) = qF_s z = \frac{q^2 n_s}{\varepsilon_w} z. \tag{A1}$$

The first step is to relate the electric field, F_s, with the subband energy values, E_i, through the one-dimensional time-independent Schroedinger equation

$$-\frac{\hbar^2}{2m_j^*}\frac{d^2\phi_i(z)}{dz^2} + V(z)\phi_i(z) = E_i\phi_i(z) \tag{A2}$$

where m_j^* is the electron effective mass in the well ($j = w$) or in the barriers ($j = b$) and ϕ_i is the wavefunction. Since the Aluminum content is only 17%, the well may be considered symmetric. Equation (A2) leads to a transcendental equation relating the electric field with the subband energies [22]

$$A_i(\alpha_+)B_i(\alpha_-) - B_i(\alpha_+)A_i(\alpha_-) = 0. \tag{A3}$$

Here $A_i(x)$ and $B_i(x)$ denote Airy functions of first and second kind, respectively, with the arguments

$$\alpha_\pm = \left(\frac{-\pi^3\hbar^2}{2qm_w^* L_{weq}^2 F_s}\right)^{2/3}\left(\frac{2m_w^* L_{weq}^2 E_i}{\hbar^2\pi^2} \pm \frac{qm_w^* L_{weq}^3 F_s}{\hbar^2\pi^2}\right). \tag{A4}$$

Equation (A3) is valid for an infinite well. The finite depth of the channel was taken into account by introducing an equivalent well width, L_{weq}, which provides the correct eigenvalues energies for the finite well of interest [22].

The energy levels for the ground and first excited states in the well as a function of the electric field are shown in Fig. 13. These results, together with (A1), are utilized to solve (9) numerically for the E_f-n_s relationship valid for pseudomorphic structures. The dependence of carrier concentration on the Fermi level is displayed in Fig. 3 for devices with square wells of width 50 and 90 Å.

ACKNOWLEDGMENT

The authors would like to thank L. F. Lester (Martin Marietta) and G. Jackson (Raytheon) for providing the HEMT's used in the experiments, and A. Rothwarf and B. Nabet for several valuable discussions.

REFERENCES

[1] C. Y. Chen, A. Y. Cho, C. G. Bethea, P. A. Garbinski, Y. M. Pang, B. F. Levine, and K. Ogawa, "Ultrahigh speed modulation-doped heterostructure field effect photodetector," *Appl. Phys. Lett.*, vol. 42, pp. 1040–1042, June 1983.

[2] C. Y. Chen, Y. M. Pang, A. Y. Cho, and P. A. Garbinski, "New minority hole sinked photoconductive detector," *Appl. Phys. Lett.*, vol. 43, pp. 1115–117, Dec. 1983.

[3] T. Umeda, Y. Cho, and A. Shibatomi, "Picosecond HEMT photodetector," *Jpn. J. Appl. Phys.*, vol. 25, pp. L801–L803, Oct. 1986.

[4] M. Z. Martin, F. K. Oshita, M. Matloubian, H. R. Fetterman, L. Shaw, and K. L. Tan, "High-speed optical response of pseudomorphic InGaAs high electron mobility transistors," *IEEE Photon. Technol. Lett.*, vol. 4, pp. 1012–1014, Sept. 1992.

[5] P. C. Clapsy and K. B. Bhasin, "Microwave response of a HEMT photoconductive detector," *Microwave Opt. Technol. Lett.*, vol. 2, pp 1–3, Jan. 1989.

[6] S. Banba, E. Suematsu, and H. Ogawa, "Fundamental properties of HEMT photodetectors for use in fiber optic links," in *Proc 23rd. European Microwave Conf.*, Madrid, Sept. 1993.

[7] A. Bangert, J. Rosenzweig, M. Ludwig, W. Bronner, P. Hofmann, and K. Kohler, "Optical Response of a Pseudomorphic HFET up to 10 GHz," in *Proc. IEEE Int. Microwave Symp.*, San Diego, May 1994.

[8] C. Rauscher and K. J. Williams, "Heterodyne reception of millimeter-wave modulated optical signals with an InP based transistor," *IEEE Trans. Microwave Theory Tech.*, vol. 42, pp. 2027–2034, Nov. 1994.

[9] C. S. Chang, H. R. Fetterman, D. Ni, E. Sovero, B. Mathur, and W. J. Ho, "Negative photoconductivity in high electron mobility transistors," *Appl. Phys. Lett.*, vol. 51, pp. 2233–2235, Dec. 1987.

[10] A. Thomasian, N. L. Sanders, L. G. Hipwood, and A. A. Rezazadeh, "Mechanism of kink effect related to negative photoconductivity in AlGaAs/GaAs HEMTs," *Electron. Lett.*, vol. 25, pp. 738–739, May 1989.

[11] M. A. Romero and P. R. Herczfeld, "Negative photoresponse in modulation doped field-effect transistors," *IEEE Trans. Microwave Theory Tech.*, vol. 43, pp. 511–517, Mar. 1995.

[12] M. A. Romero, "Modulation doped field-effect photodetectors," Ph.D. dissertation, Drexel Univ., June 1995.

[13] A. Singhal, A. Mishra, and P. Chakrabarti, "Optical effects in modulation doped field effect transistors," *Solid State Electronics*, vol. 33, pp. 1214–1216, Sept. 1990.

[14] A. A. A. de Salles, "Optical effects in HEMTs," *Microwave Opt. Technol. Lett.*, vol. 3, pp. 350–354, Oct. 1990.

[15] A. A. A. de Salles and M. A. Romero, "AlGaAs/GaAs HEMT's under optical illumination," *IEEE Trans. Microwave Theory Tech.*, vol. 39, pp. 2010–2017, Dec. 1991.

[16] A. Madjar, A. Paolella, and P. R. Herczfeld, "Analytical model for the optically generated currents in GaAs MESFET's," *IEEE Trans. Microwave Theory Tech.*, vol. 40, pp. 1681–1691, Aug. 1992.

[17] C. Kocot and C. A. Stolte, "Backgating in GaAs MESFETs," *IEEE Trans. Electron Devices*, vol. 29, pp. 1059–1064, July 1982.

[18] S. Subramanian, D. Schulte, L. Ungier, P. Zhao, T. K. Plant, and J. R. Arthur, "A high-gain modulation doped photodetector using low temperature MBE grown GaAs," *IEEE Electron Device Lett.*, vol. 16, pp. 20–22, Jan. 1995.

[19] M. Shur, *Physics of Semiconductor Devices*. Englewood Cliffs, NJ: Prentice-Hall, 1990.

[20] R. J. Krantz and W. L. Bloss, "The role of acceptor density on the high channel carrier density I–V characteristics of AlGaAs/GaAs MODFETs," *Solid State Electron.*, vol. 33, pp. 941–945, July 1990.

[21] T. J. Drummond, H. Morkoc, K. Lee, and M. Shur, "Model for modulation doped field effect transistor," *IEEE Electron Device Lett.*, vol. 3, pp. 338–340, Nov. 1982.

[22] D. A. B. Miller, D. S. Chemla, T. C. Dammen, A. C. Gossard, W. Wiegmann, T. H. Wood, and C. A. Burrus, "Electric field dependence of optical absorption near the band gap of quantum-well structures," *Phys. Rev. B*, vol. 32, pp. 1043–1060, July 1985.

[23] E. Garmire, N. M. Jokerst, A. Kost, A. Danner, and P. D. Dapkus, "Optical nonlinearities due to carrier transport in semiconductors," *J. Opt. Soc. Amer. B.*, vol. 6, pp. 579–587, Apr. 1989.

[24] Y. Ando and T. Itoh, "Analysis of charge control in pseudomorphic two-dimensional electron gas field-effect transistors," *IEEE Trans. Electron Devices*, vol. 35, pp. 2295–2301, Dec. 1988.

Murilo A. Romero was born in Rio de Janeiro, Brazil, in 1965. He received the B.Sc. and M.Sc. degrees from Pontifical Catholic University of Rio de Janeiro, in 1988 and 1991, respectively, both in electrical engineering. In 1995, he received the Ph.D. degree from Drexel University, Philadelphia, PA, under a fellowship from the Brazilian Research Council (CNPq). His thesis topic was the modeling of microwave transistors under optical illumination.

Since 1995, he has been an Assistant Professor, University of Sao Paulo, Sao Carlos, Brazil. His current research interests are optical fiber sensors, nonlinear photonics, and the modeling and simulation of optoelectronic semiconductor devices and circuits.

M. A. G. Martinez was born in Rio de Janeiro, Brazil, in 1965. She received the B.Sc. and M.Sc. degrees in electrical engineering from the Catholic University of Rio de Janeiro in 1988 and 1991, respectively. She is currently pursuing the Ph.D. degree at Drexel University, Philadelphia, PA. Her research interests are the modeling of reduced dimentionality optoelectronic devices and nonlinear optics.

Peter R. Herczfeld was born in Budapest, Hungary, in 1935. He received the B.Sc. degree in physics from Colorado State University, Fort Collins, in 1961, the M.Sc. degree in physics in 1963, and the Ph.D. degree in electrical engineering in 1967, both from the University of Minnesota, Minneapolis.

Since 1967, he has been the faculty of Drexel University, Philadelphia, PA, where he is a Professor of Electrical and Computer Engineering. He has published over 300 papers in solid-state electronics, microwaves, photonics, solar energy, and biomedical engineering. He is the Director of the Center for Microwave-Lightwave Engineering at Drexel University, a Center of Excellence that conducts research in microwave and photonics. He has served as project director for more than 70 projects.

Dr. Herczfeld, a member of APS, SPIE and the ISEC, is a recipient of several research and publication awards, including the Microwave Prize (16 and 1994).